NBSIR 80-2047

Application of Fracture Mechanics in Assuring Against Fatigue Failure of Ceramic Components

J. E. Ritter, Jr.

Mechanical Engineering Department
University of Massachusetts
Amherst, MA 01003

S. M. Wiederhorn, N. J. Tighe and E. R. Fuller, Jr.

National Bureau of Standards
Fracture and Deformation Division
National Measurement Laboratory
Center for Materials Science
U.S. Department of Commerce
Washington, DC 20234

June 1980

Prepared for

epartment of Energy
ssil Fuel Utilization Division
ashington, DC

NBSIR 80-2047

APPLICATION OF FRACTURE MECHANICS IN ASSURING AGAINST FATIGUE FAILURE OF CERAMIC COMPONENTS

J. E. Ritter, Jr.

Mechanical Engineering Department
University of Massachusetts
Amherst, MA 01003

S. M. Wiederhorn, N. J. Tighe and E. R. Fuller, Jr.

National Bureau of Standards
Fracture and Deformation Division
National Measurement Laboratory
Center for Materials Science
U.S. Department of Commerce
Washington, DC 20234

June 1980

Prepared for
Department of Energy
Fossil Fuel Utilization Division
Washington, DC

U.S. DEPARTMENT OF COMMERCE, Philip M. Klutznick, *Secretary*

Luther H. Hodges, Jr., *Deputy Secretary*
Jordan J. Baruch, *Assistant Secretary for Productivity, Technology, and Innovation*

NATIONAL BUREAU OF STANDARDS, Ernest Ambler, *Director*

APPLICATION OF FRACTURE MECHANICS IN ASSURING AGAINST FATIGUE FAILURE OF CERAMIC COMPONENTS

J. E. Ritter, Jr.

University of Massachusetts
Amherst, MA. 01003

S. M. Wiederhorn, N. J. Tighe and E. R. Fuller, Jr.

Fracture and Deformation Division
National Bureau of Standards
Washington, D. C. 20234

INTRODUCTION

The use of ceramics in high performance applications offers a challenge to scientists and engineers: the challenge of designing structural components with brittle materials. Design problems arise for two reasons when brittle materials are used as structural components: 1. The strength of brittle materials is not a well defined quantity, but can vary widely depending on the material; 2. The strength of brittle materials is time dependent so that these materials often exhibit a time delay to failure. This time dependence and scatter of strength so typical of most ceramic materials occurs because of the presence of defects such as cracks or crack-like flaws in these materials. When subjected to an applied tensile stress, these defects act as stress concentrators and fracture occurs when the applied stress intensity factor reaches a critical value. Scatter in the strength of ceramic materials is a consequence of the scatter in the size of the most critical defect in the ceramic. The time dependence of strength results from subcritical crack growth which gradually lengthens the crack until it reaches critical dimensions, at which time failure occurs. The time delay to failure is the time required for the crack to go from a subcritical to a critical size.

Methods of dealing with design problems involving fatigue of ceramic materials have been developed over the past 10 years through the application of the techniques and concepts of fracture mechanics (1-3). Since fracture mechanics techniques can be used to characterize both the conditions for subcritical crack growth and the conditions for crack instability, they can be used for purposes of design to estimate the allowable applied stress and the expected lifetime for a given component. This is accomplished by estimating the initial crack size in a ceramic component and the time required for the crack to grow from its initial size to a final critical size. Several mutually independent techniques have been developed recently to provide these types of estimates. Since these techniques promise to revolutionize the way in which structural components made of ceramic materials are designed, a complete understanding of these techniques, their application, and their limitations will be necessary to use them correctly.

This paper will review the application of fracture mechanics theory to the prevention of delayed failure of ceramics. Three successful applications of this theory of assuring the mechanical reliability of ceramics are discussed in order to demonstrate the viability of the theory for purposes of engineering design. Finally, a description is presented of practical limitations of the theory with regard to heat engine application. Methods of overcoming these limitations through modification of test procedures, and application of statistical theory are then presented.

THEORY

Since fracture mechanics concepts can be used to characterize both the conditions for subcritical crack growth and the conditions for crack instability, they can be used to predict the failure of ceramic materials under given service conditions. This is accomplished by estimating the initial crack size in a ceramic component and the time for the crack to grow from its initial size to a final critical size. As the crack grows to its critical size, the crack velocity (V) is assumed to be dependent on the applied stress intensity factor (K_I) by (1):

$$V = A K_I^N \tag{1}$$

where A and N are crack growth constants that depend on the environment and material composition. From Equation (1) and the relation $\sigma=K_{IC}/Y\sqrt{a}$, it can be shown that the time to failure (t_f) under constant applied tensile stress (σ_a) is (3):

$$t_f = B S^{N-2} \sigma_a^{-N} \tag{2}$$

where $B = 2/(AY^2(n-2)K_{IC}^{N-2})$, K_{IC} = critical stress intensity factor, and S = fracture strength in an inert environment where no subcritical crack growth occurs prior to fracture. From its definition, B is a crack propagation constant that depends on the environment and material composition.

In Equation (2), t_f represents the time required for a flaw to grow from an initial, subcritical size, to dimensions critical for catastrophic propagation; B and N are the constants that characterize this subcritical crack growth. The initial flaw size is characterized in Equation (2) by the fracture strength in an inert environment*. From Equation (2) it is seen that the time to failure decreases with increasing stress, i.e. fatigue under a static stress.

Also from Eq. (1), a relationship can be derived between the fracture strength σ_f and stressing rate $\dot{\sigma}$. In this case flaws grow from subcritical to critical size under constantly increasing stress. The results of this analysis is (1-3):

$$\sigma_f^{N+1} = B\,(N+1)\,S^{N-2}\,\dot{\sigma} \qquad (3)$$

where B and N are the same fatigue constants as in Eq. (2). From Equation (3) it is seen that fracture strength decreases with decreasing stressing rate since the flaws have more time to grow. This behavior is known as dynamic fatigue, i.e. fatigue under constant stressing rate conditions.

The probability of failure (F) for a given lifetime and applied stress can be obtained from Equation (2) by expressing the inert strength in terms of its failure probability distribution. Generally, the inert strength distribution of ceramics can be approximated by the Weibull relationship (3):

$$\ln \ln \frac{1}{1-F} = m \ln \frac{S}{S_o} \qquad (4)$$

where m and S_o are empirical constants evaluated by a fit of the strength data. Likewise, the strength distribution at a fixed stressing rate can be obtained by substituting Equation (4) into Equation (3).

Because ceramics exhibit a wide spread in strength values (m is typically 4-8), the allowable stress in service is quite

*The initial crack size, a, can be calculated, if desired, from the well known fracture mechanics relationship: $a = K_{IC}^2/Y^2S^2$, where Y is a constant that is determined by the geometry of the specimen and the crack. In subsequent discussion, a is assumed to be small relative to component dimensions so that Y is a single valued constant.

low if low failure probabilities are required. Proof testing offers one means of increasing the design stress for ceramics (1-3). The value of proof testing is that it characterizes the largest effective flaw possible in a tested component, since any larger flaws would have caused failure during the proof test.

Assuming that flaw growth during the proof test cycle is given by Equation (1) (i.e. one region of crack growth) and that the initial inert strength distribution can be characterized by Equation (4), the inert strength after proof testing (S_a) is given by (4):

$$(S_a/S_o)^{N_p-2} = (-\ln(1-F_a)-\ln(1-F_p))^{(N_p-2)/m} - (-\ln(1-F_p))^{(N_p-2)/m} + (S_{min}/S_o)^{N_p-2} \quad (5)$$

where N_p is the crack propagation constant appropriate for the proof test environment, F_a is the failure probability after proof testing, F_p is the failure probability of the proof test and S_{min} is the minimum inert strength of a sample that just passes the proof test cycle, i.e. the truncation strength. It is significant to note that the inert strength after proof testing is truncated at S_{min} and will be greater than the initial inert strength at all levels of failure probability if $m < N_p-2$ (4).

For a given material and proof test environment, S_{min} is determined only by the unloading rate ($\dot{\sigma}_u$) from the proof stress (4):

$$S_{min} = [\dot{\sigma}_u B_p (N_p-2)]^{1/3} [3/(N_p+1)]^{1/(N_p-3)} \quad (6)$$

where B_p is the crack propagation constant appropriate for the proof test environment. If $\dot{\sigma}_u > 0$, Equation (6) shows that proof testing always truncates the strength distribution. The higher $\dot{\sigma}_u$, the greater is the strength level, S_{min}, at which truncation occurs. However, since S_{min} cannot be greater than the maximum stress, σ_p, during the proof test, σ_p is an upper bound for S_{min}. Substitution of σ_p for S_{min} in Equation (6) gives the minimum unloading rate for which σ_p is approximately equal to the truncation strength. Equation (6) also shows that good proof test conditions (high N_p) result in a high S_{min}.

The failure probability of the proof test (F_p) can be determined directly from the number of specimens that break during the proof test or can be predicted from (4):

$$-\ln(1-F_p) = (S_o^m)^{-1} (D_p/B_p)^{m/(N_p-2)} \quad (7)$$

where $D_p = \int_o^t \sigma_p^{N_p}(t)\,dt$ represents the amount of strength degradation during the proof stress cycle. For a typical proof test, the component is loaded at a constant rate, $\dot{\sigma}_1$, held at the maximum proof stress, σ_p, for a time t_p, and then unloaded at a constant rate, $\dot{\sigma}_u$. Integrating the D_p equation for this typical proof stress cycle gives:

$$D_p = \sigma_p^{N_p} t_p + [\sigma_p^{N_p+1}/(N_p+1)]\,(1/\dot{\sigma}_u + 1/\dot{\sigma}_1) \qquad (8)$$

By coupling Equation (5) with Equations (2) and (3), the t_f and σ_f distribution after proof testing can be predicted for any service environment (4). Of particular interest is the minimum lifetime (t_{min}) in service of a component after proof testing. This is obtained by substituting S_{min} for S in Equation (2) so that:

$$t_{min} = BS_{min}^{N-2}\sigma_a^{-N} \qquad (9)$$

where now B and N are the appropriate crack parameters for the service environment.

Equations (5) - (9) summarize failure predictions for ceramic materials after proof testing. These failure predictions are dependent on the crack propagation parameters B and N. These parameters must be determined in a test environment that simulates the appropriate proof-test and service conditions and can be obtained from one of three type of experiments: crack velocity experiments, stress rupture experiments, and stressing rate experiments (3). From crack velocity experiments, Equation (1) is used to determine A and N; K_{IC} is determined in a separate experiment. Stress rupture data (t_f vs. σ_a) and the inert strength data are used to determine B and N from Equation (2), whereas stressing rate data (S vs. $\dot{\sigma}$) and median inert strength data are used to calculate B and N from Equation (3). The stress rupture and stressing rate techniques are commonly referred to as static fatigue and dynamic fatigue, respectively.

APPLICATION

The fracture mechanics principles described in the previous section have been experimentally verified for soda-lime glass (3) and alumina (5) in a moist environment. Specifically, these studies showed that the three experimental techniques for measuring the crack propagation parameters B and N give equivalent results, that the time-to-failure and strength failure probability distributions can be predicted from Equations (2) and (3) coupled with Equation (4), and that strength distributions after proof

testing can be predicted on the basis of Equation (5). The purpose of this section is to describe three applications of fracture mechanics principles in assuring against the fatigue failure of ceramic components in service.

Failure Statistics

For alumina substrates fabricated by cofired metallurgy, stress corrosion cracking can be a serious problem. The metals most commonly cofired with alumina are either molybdenum or tungsten. Because these metals possess lower thermal expansion coefficients than alumina, their cosintering can cause the ceramic to retain residual tensile stresses of considerable magnitude. Subsequent cleaning and plating baths, necessary to render the metallurgy solderable, expose the substrate to conditions that promote stress corrosion cracking in the alumina. To statistically assess the susceptibility of polycrystalline

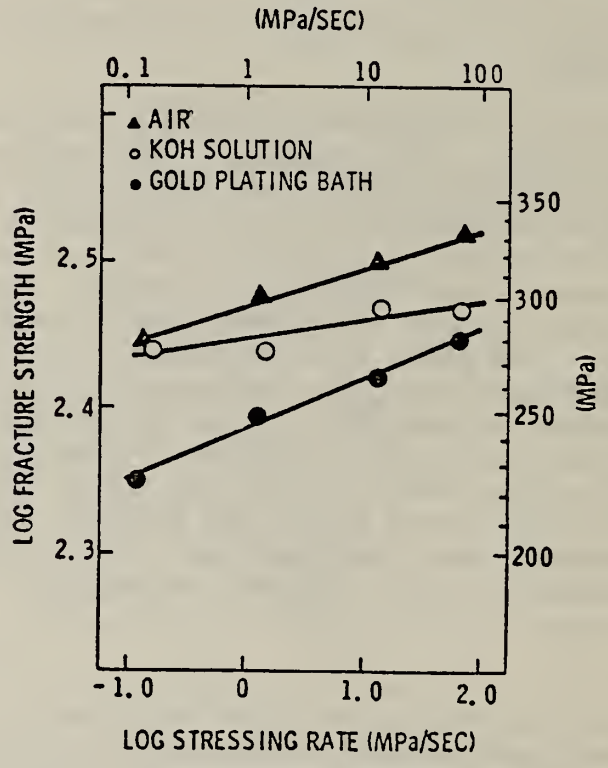

Figure 1. Dynamic fatigue data of polycrystalline alumina in a KOH cleaning solution at 100°C, in a gold-plating bath at 78°C, and in moist air at 30°C and 80% RH (from Ref. 6).

alumina to stress corrosion cracking under processing conditions, the stressing rate technique was used to characterize the crack propagation parameters for alumina in a KOH cleaning solution at 100°C and a gold plating solution at 78°C (6).

Figure 1 gives the experimental results of strength as a function of stressing rate of alumina in the KOH and gold solutions (6). For comparison, the fatigue strength results determined for the same alumina in a moist air environment are included (5). From this data and a knowledge of the inert strength of the samples, the crack propagation parameters B and N were determined from Equation (3) for the various environments.

To validate the applicability of fracture mechanics principles in predicting failure probability in the processing solutions, the actual fatigue strength distributions were compared to predictions based on Equation (3) using the appropriate values for B and N and the inert strength distribution of the samples. Figure 2 gives these comparisons and it is evident that agreement between the theoretical predictions and the actual fatigue strength distributions

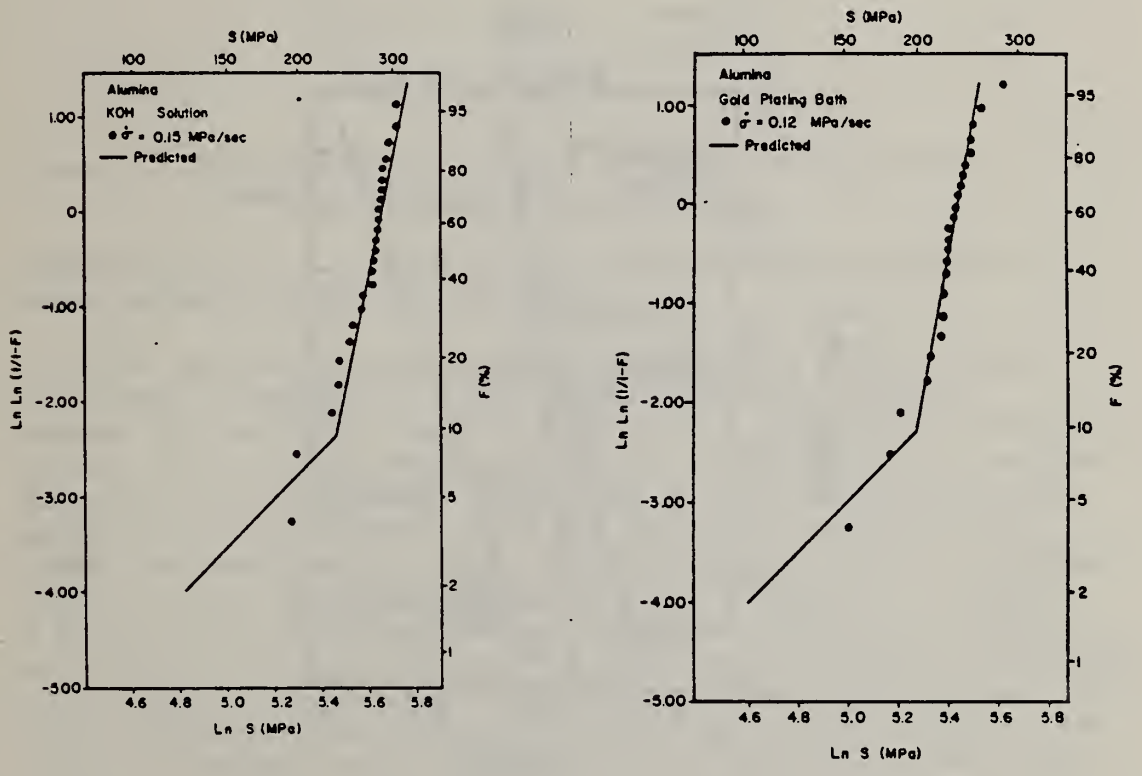

Figure 2. Comparison to theoretical predictions of the strength distributions of polycrystalline alumina in a) KOH cleaning solution at 100°C and b) gold plating bath at 78°C (from ref. 6).

is good. It should also be noted that these strength distributions are bimodal since the low strength regime of the distribution was caused by gross flaws induced in the samples during grinding.

The severity of the processing conditions on the alumina substrates can be most easily assessed by means of a lifetime prediction diagram (Figure 3) based on Equation (2) and the inert strength distribution of the substrates. Although the strengths of the substrates could not be measured directly, they were estimated from the strength distribution of the samples and the Weibull size relation:

$$S_1 = S_2 \, (A_2/A_1)^{1/m} \tag{10}$$

where S_1 and S_2 are the strengths of the substrates and samples, respectively, and A_1 and A_2 are the surface area of the substrates and samples, respectively.[2] Figure 4 shows the estimated inert strength distribution of the substrates. It should be noted that it was assumed that the inert strength distribution of the

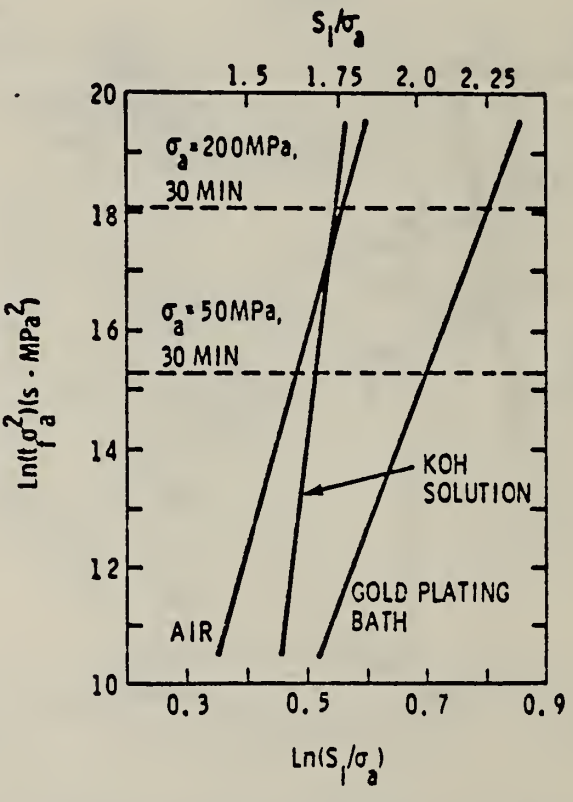

Figure 3. Lifetime prediction diagram for polycrystalline alumina in wet processing environments and moist air (from ref. 6).

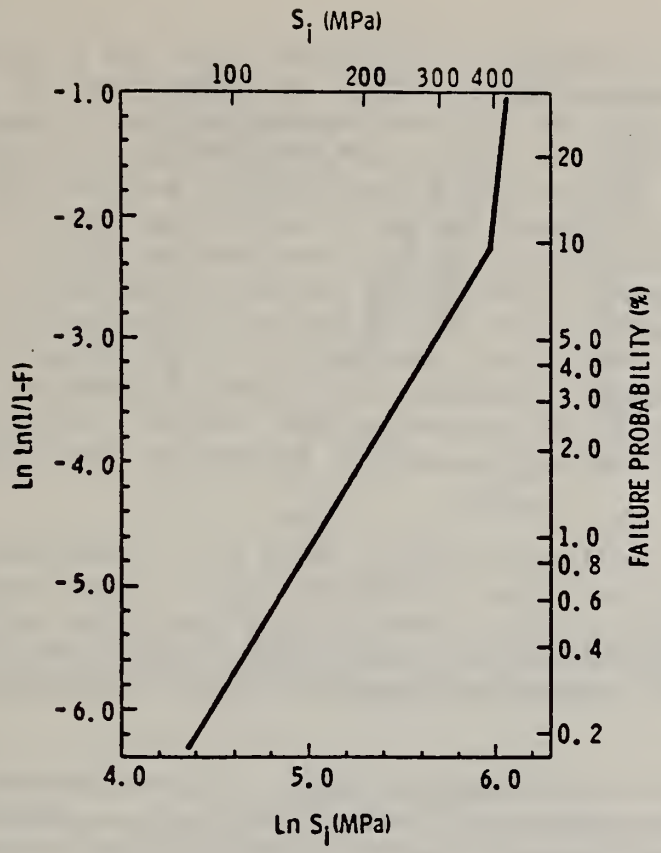

Figure 4. Estimated Weibull inert strength distribution for alumina substrates (from ref. 6).

substrates was not altered through any interaction between the metal and alumina during sintering.

The residual tensile stress in a substrate having cofired metallurgy is dependent on the thermal expansion mismatch between the metallurgy and the ceramic, the temperature difference between the set point of the system and room temperature, and the geometry of the metallurgy in the system. In molybdenum-alumina substrates residual stresses of 200 MPa can be generated. If substrates having such stresses are subjected to the KOH cleaning solution or the gold-plating solution for 30 minutes, respective S/σ_a ratios of 1.75 and 2.27 are predicted (Figure 3). Since σ_a is known, S can be calculated and a failure probability determined from Figure 4. With a 200 MPa residual stress, an 8% failure rate would be expected for the substrates in the 10% KOH solution, and 40% of the substrates in the gold-plating bath would crack after 30 minutes. Also, substrates having a residual stress of this magnitude would have a failure rate of 8% in hot, humid air. Clearly, failure rates of this magnitude are unacceptable.

The failure probability of the substrates can be lowered by: (1) using a stronger alumina to make the substrates, (2) reducing the processing times, or (3) reducing the residual stress in the substrates. The obvious choice is to reduce the residual stress in the ceramic. This can be accomplished by reducing the thermal expansion mismatch between the metal and the ceramic, by altering the geometry of the system, or by a combination of both. Since the thermal expansion differential can be reduced only by altering the metal configuration and/or the ceramic, this choice alone is not particularly attractive. Similarly, if the stress is lowered only through geometric redesign, the potential geometric density of the metallurgy in the system becomes limited. Thus, a combination of both approaches is generally considered most effective in reducing stress.

Obviously, the ideal solution would be to completely eliminate any residual tensile stress in the substrates; this, however, is not always possible without drastically altering the material system. The problem then is to reduce the failure probability of the substrates to a magnitude compatible with good product reliability.

Regardless of the technique used, if the stress in the ceramic is lowered, for instance, to 50 MPa, the lifetime prediction diagram and the inert strength distribution can again be used to assess the probability of stress corrosion cracking of the substrates. If substrates having a residual stress of 50 MPa are placed in the KOH cleaning solution or in the gold plating bath for 30 minutes, it can be determined from Figure 3 and 4 that the failure probabilities are 0.2 and 0.34% respectively. While the possibility of stress corrosion cracking of substrates during processing is not completely eliminated by reducing the residual stress to 50 MPa, the resultant failure rates are now low enough so as to offer a minimal impact on product reliability.

The above examples of lifetime predictions serve to illustrate the importance of fracture mechanics theory in designing electronic substrates fabricated by cofired metallurgy, namely, that substrates of various designs can be compared for the probability of stress corrosion cracking due to the residual tensile stress in the substrates. In this way, fracture mechanics theory is useful in making more rational design decisions. These predictions can also be checked by fabricating substrates of several designs with different residual stresses, and then subjecting the substrates, for instance, to the gold-plating bath for a given period of time. By comparing the incidence of stress corrosion cracking with that predicted by fracture mechanics theory, the theory can be experimentally validated. This was done in the present research program, and the experimental results generally agreed with those theoretically predicted (6).

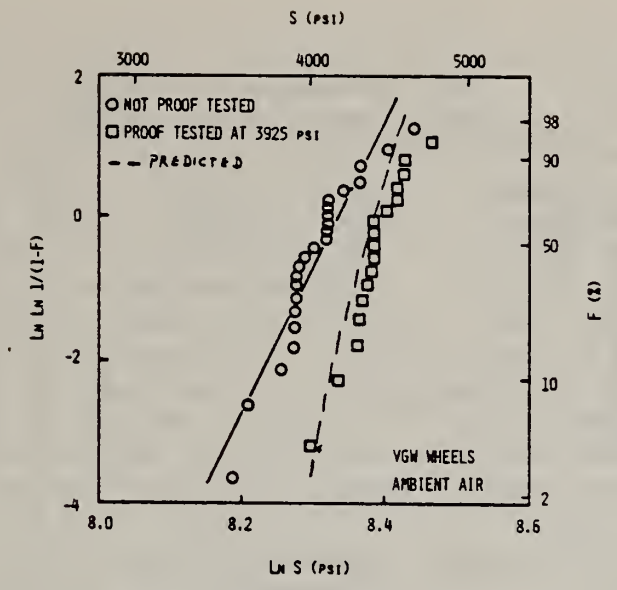

Figure 6. Comparison of wheel bursting strengths before and after proof testing for wheel specification VGW2 (from ref. 7).

characterize the strength and fatigue behavior of ceramics at elevated temperatures to establish allowable stress levels for component design. To study the high temperature strength and fatigue behavior of high purity alumina (Wesgo AL 995) the stressing rate test technique was used because of its simplicity (8).

The effect of temperature on the strength and fatigue behavior of high purity alumina is given in Figure 7 (8). The temperature dependence of both strength and fatigue behavior is small up to 500°C. From 800 to 1100°C both the strength and fatigue resistance decreases markedly. A convenient way to show the effects of fatigue is to compare minimum lifetime predictions, based on Equation (9) taking S_{min} to be equal to σ_p, as a function of temperature. Figure 8 gives these predictions and clearly illustrates that there is little difference in the fatigue behavior of high purity alumina from 23 to 500°C; however at higher temperatures fatigue effects become very important. For example, to assure a minimum lifetime of one year under a service stress of 100 MPa the required proof stress ratio is 2.27 for a temperature of 23°C but for 1000°C it is 6.90 and for 1100°C it is 14.91. These elevated temperature proof stress ratios would result in such large proof stresses that no sample would be able to pass the proof test. To get more reasonable proof stresses, the expected minimum life or allowable stress in service must be decreased for these elevated temperatures. For example, if the allowable stress is reduced to 30 MPa, then the proof stress to insure a minimum lifetime of 1 year at 1000°C is 179 MPa and 361 MPa at 1100°C.

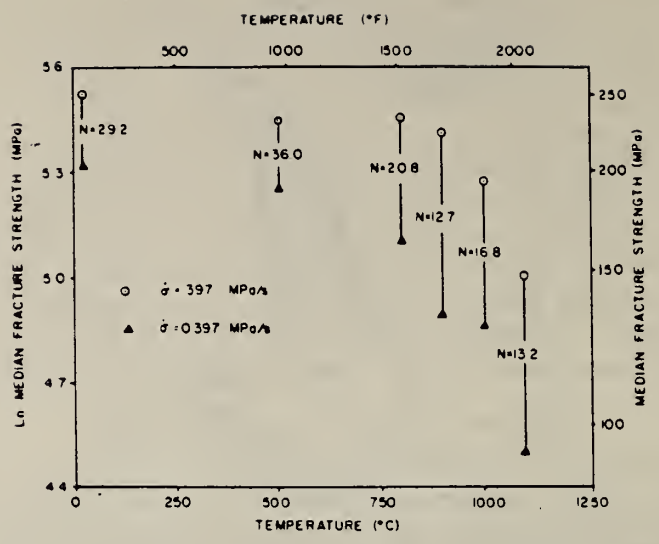

Figure 7. Median fracture strength of alumina as a function of temperature and stressing rate (from ref. 8).

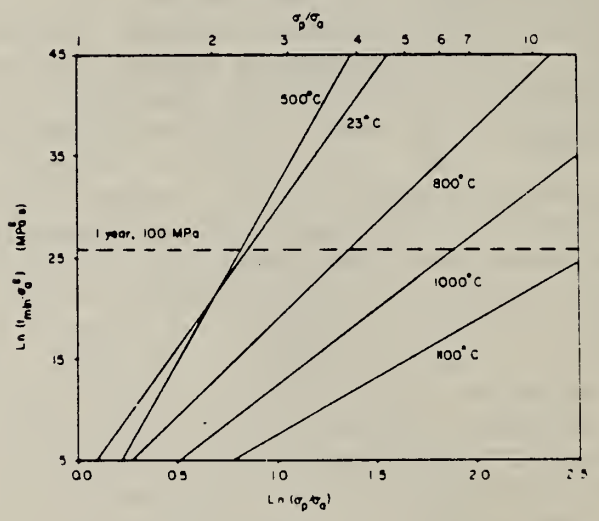

Figure 8. Minimum lifetime prediction diagram for alumina as a function of temperature (from ref. 8).

Scanning electron micrographs showed that the fracture in this high purity alumina changed from transgranular at 23°C to intergranular at temperatures above 800°C (8). In addition, a glassy phase was found at the fracture origins of the samples tested at above 800°C, giving evidence that the glassy phase is playing a major role in determining the strength and fatigue behavior of high purity alumina at elevated temperatures. However, proof test results (8) showed that the preexisting flaw population is not altered at elevated temperatures. Figure 9 compares the strength distribution of alumina at 23 and 1100°C before and after proof testing at room temperature. It is evident that this proof test eliminated the weak samples so that the after proof strength distribution at low failure probabilities are stronger than the initial distributions and that agreement between theory and experiment is good. On the other hand, Figure 10 shows that proof testing alumina at 1000°C is not effective in improving the strength distribution at 1000°C; however, the good agreement between experiment and theory gives evidence that fracture mechanics theory applies. In this case weak samples are eliminated by proof testing at 1000°C, but flaw growth during the proof test weakens the survivors to such a degree that proof testing is not effective in improving the strength distribution.

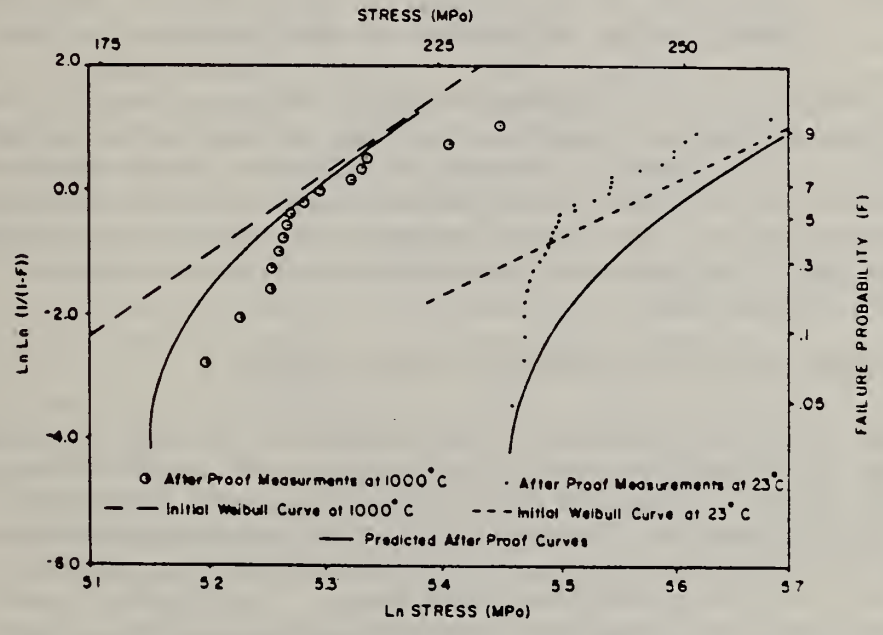

Figure 9. Effect of room temperature proof testing on the strength distribution of alumina at 23°C and 1000°C (from ref. 8).

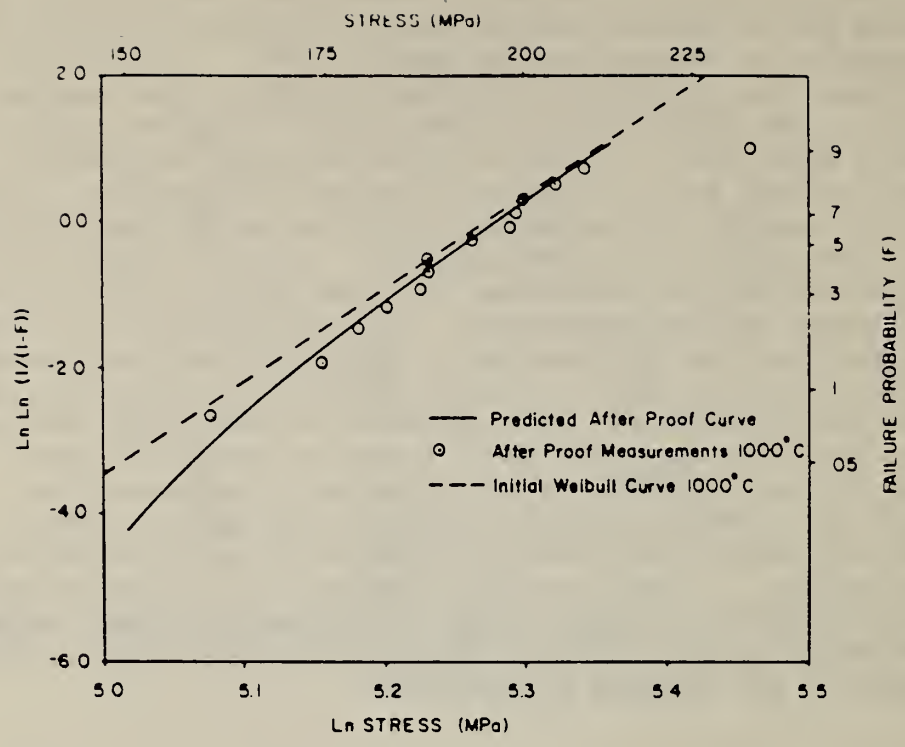

Figure 10. Effect of proof testing at 1000°C on the strength distribution of alumina at 1000°C (from ref. 8).

In summary, it is believed that at moderate temperatures the fatigue failure of alumina is caused by moisture assisted subcritical crack growth; whereas, at elevated temperatures it is caused by subcritical crack growth enhanced by the presence of a glassy phase. It is also thought that the same pre-existing flaws control the strength both at room temperature and at elevated temperatures.

LIMITATIONS OF THE LIFETIME PREDICTION METHOD

The lifetime prediction theory presented in this paper is based on the assumption that subcritical crack growth from pre-existing flaws is the only mechanism of strength degradation. Using this assumption, component lifetime can be predicted once the initial flaw population, the crack growth rate and the critical crack size have been determined. The theory is deterministic because the element of chance is eliminated from the lifetime prediction once these parameters have been evaluated. The accuracy of the lifetime prediction will depend on both the accuracy with which the pertinent parameters can be evaluated (9-11), and the adequacy of the crack growth equation (12). This requirement does not detract from the basic deterministic nature of the method. The prediction scheme can, however, be

invalidated when the basic assumptions of the theory are not satisfied. Thus, fracture processes, other than subcritical crack growth, can invalidate failure predictions based on this theory. Unfortunately, other fracture processes do occur for materials currently under consideration for use in heat engines, so that alternate mechanisms of failure must be considered for any scheme of predictive failure for heat engine components. As will be shown, proper modeling of these factors permits extension of the theory to handle fracture situations that are not currently included in the method of lifetime prediction.

As with most other ceramic materials, silicon nitride and silicon carbide fail at low temperatures from preexisting flaws. As discussed by Rice et al. (13,14) and by Richerson and Yonushonis (15), these flaws are usually surface cracks introduced into silicon nitride and silicon carbide components by machining when the components are manufactured. For hot-pressed silicon nitride at temperatures less than $\sim$1000°C, fracture originates from surface flaws in a completely brittle manner (13,14). At higher temperatures, however, plasticity of components and effects resulting from the reactive nature of the test environment intervene to alter the mode of fracture (13). The same types of effects occur for hot-pressed silicon carbide at higher temperatures ($\sim$1400°C). In oxidizing environments, the effects of temperature on mechanical behavior can be attributed to: (1) enhanced plasticity at the crack tip which results in subcritical crack growth by creep fracture (16,17), and (2) surface oxidation which results in the healing of surface machining cracks, and for some materials, the generation of new flaws that act as new origins for fracture (13-15, 18-20). Both processes have to be considered to accurately predict the lifetime of high temperature structural components. A variety of other processes (thermal shock, particle impact, chemical corrosion, component contacts, etc.) can also intervene to effect the fracture behavior of heat engine ceramics. Although a complete theory of failure would require all of these processes to be considered, such extensive considerations are clearly beyond the scope of this paper. The discussion in the remainder of this paper will be more limited in scope, dealing with pit formation, crack healing and crack growth. Materials to be considered are magnesia-doped, hot-pressed, silicon nitride and reaction bonded silicon nitride for which the processes that occur at elevated temperatures are best understood.

High temperature oxidation has been shown to be particularly effective in altering the initial flaw population in hot-pressed, silicon nitride (NC132). Investigations of the strength and oxidation behavior of this material have shown that surface induced machining flaws are reduced in severity by high temperature oxidation of the ceramic surface (13-15, 18-20). The

oxidation process is complex involving mass transport of impurities from the matrix, and transport of oxygen and nitrogen through the glass oxide layer that forms on the surface of the ceramic (17,21). As the oxide scale grows, the initial silicon nitride surface recedes, reducing the size of the surface cracks and thus their severity (Figure 11). If oxidation continues long enough, the surface cracks can be completely removed from the ceramic surface. In addition to crack removal by dissolution, plastic deformation at elevated temperatures also permits blunting of machining flaws and relief of surface stresses, thus enhancing the strength of the component (22,23). The effectiveness of oxidation in reducing flaw severity can be illustrated by the introduction of fresh cracks into the surface of silicon nitride by indentation (20,24). As illustrated in Table 2 on hot-pressed silicon nitride (billet B), exposure at 1200°C in air increased the strength from 408 MPa at room temperature to 488 MPa after 100 hours exposure, largely as a result of decreasing the severity of the flaw associated with the indentation. Because of the beneficial effect of oxidation, high temperature exposure in air is being used as a means of improving the finish of hot-pressed silicon nitride ceramic blades (15,23). Similar strengthening results are observed for reaction bonded silicon nitride (NC350) (23,24).

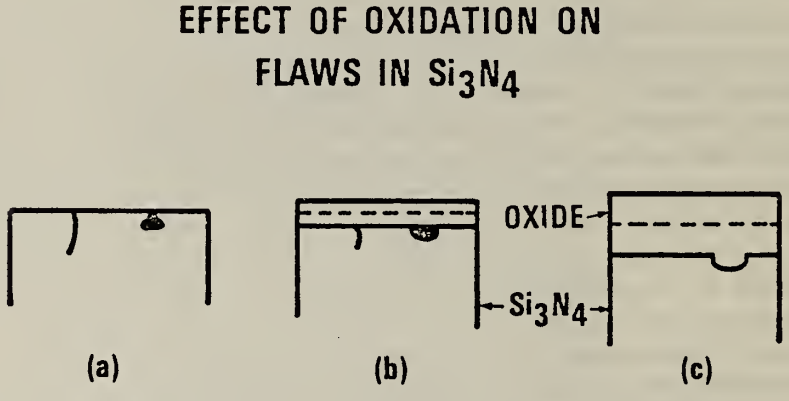

Figure 11. Effect of exposure at 1200°C on flaws in silicon nitride: (a) surface crack and subsurface inclusion before exposure; (b) after exposure crack size is reduced by surface dissolution and subsurface flaw reacts with environment. At the same time, crack blunting or crack healing occurs; (c) oxide growth has removed the subsurface crack and enlarged the subsurface flaw to produce a pit in the silicon nitride (from ref. 34).

Table 2.

Strength of Indented Specimens: 2kg Load (34)

Material	Test-Temp. °C	Exposure Conditions	Strength MPa	Fracture at indentation
NC132 Billet A	25	as indented	397 ± 12	Yes
	25	16 hr 1200°C	432 ± 27	Yes
	25	100 hr 1200°C	461 ± 42	No
	1200	1/2 hr 1200°C	438 ± 15	Yes
	1200	16 hr 1200°C	396 ± 42	Yes
	1200	100 hr 1200°C	402 ± 12	No
NC132 Billet B	25	as indented	408 ± 17	Yes
	25	100 hr 1200°C	524 ± 47	Yes
	1200	1/2 hr 1200°C	441 ± 10	Yes
	1200	100 hr 1200°C	488 ± 11	Yes
NC350	25	as indented	115 ± 24	Yes
	25	33 hr 1200°C	181 ± 22	Yes
	25	100 hr 1200°C	225 ± 38	Yes
	1200	100 hr 1200°C	188 ± 64	Yes
NCX-34 Y_2O_3	25	as indented	491 ± 16	Yes
	25	100 hr 1200°C	616 ± 51	No
	1200	100 hr 1200°C	744 ± 25	Yes

If flaw removal were the only process occurring during oxidation then the lifetime prediction methods presented earlier in this paper could be used as a conservative basis for component design. In this case, the starting flaws would decrease in size as oxidation occurred, and the component would become stronger, not weaker. Research on hot-pressed silicon nitride (NC132) has shown that flaw generation during long term (>100 hr.) exposure results in a decrease in the strength of this material (15, 20, 22). The strength decrease results from pit formation at the ceramic surface due to rapid localized oxidation. Although the exact cause of localized oxidation is not fully understood, it probably results from the presence of impurities in the ceramic which increase the oxidation rate as the oxide interface approaches the location of the impurity (Figure 11; 20,26). The formation of glass-like oxide mounds over the pits with holes in the center of the mounds suggests that rapid gas generation is associated with the nucleation and growth of these pits (20).

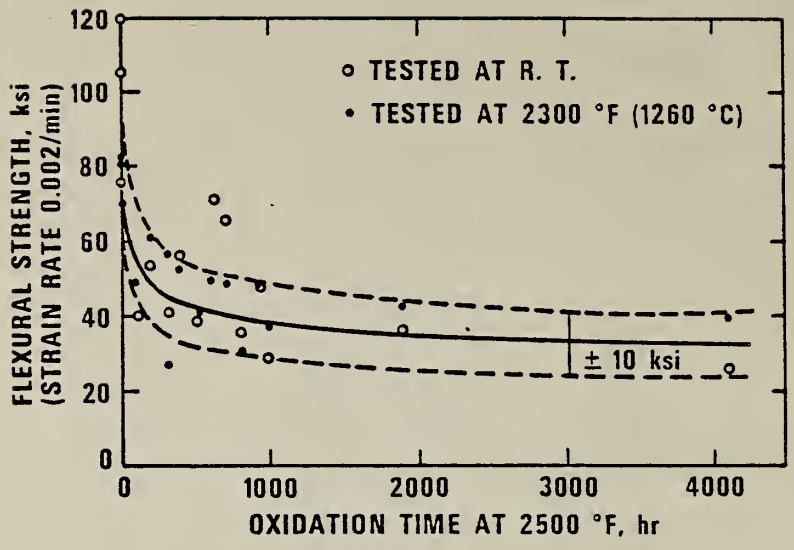

Figure 12. Effect of oxidation at 1371°C (2500°F) on the strength of silicon nitride (NC132). Note that at time zero the scatter in strength is considerably greater than that occurring after substantial periods of exposure (from ref. 25).

The effect of pit formation on the long term strength is illustrated in Figure 12 which shows that after 1000 hours exposure magnesia-doped, hot-pressed silicon nitride has lost approximately 50 percent of its strength (25). This strength decrease seems to occur most rapidly during the initial stages of exposure, suggesting rapid formation of pits initially, and then stabilization of the pit structure after periods of about 1000 hours. Whether or not the pit structure has reached a state of static equilibrium, or is in a state of dynamic equilibrium has not yet been determined.

In freshly machined specimens the combined effect of crack healing, and flaw generation should result in a strength enhancement followed by a strength degradation as pits form in the material (20,24). This type of behavior has been confirmed by a number of investigators. Richerson and Yonushonis (15) have shown, for example, that the strength of transverse ground silicon nitride is increased by exposure to temperatures of 982°C or 1066°C for 50 hours (Table 3). At higher temperatures or for longer periods of time, a strength decrease is observed as pits are formed in the surface. Wiederhorn and Tighe (20,24) showed that this type of behavior depended on the particular billet used for study, since some billets increased in strength

Table 3.

Room Temperature Strength of Hot-Pressed, Silicon Nitride (NC132) Transverse Ground Specimens Tested in 4-Point Bending (15)

Exposure °C (°F) time	Strength and Standard Deviation MPa (KSI)	Samples Tested	Predominant Fracture Region
Control	450 ± 36 (63.0 ± 5.0)	12	Grinding Groves
982 (1800) 50 hours	657 ± 61 (92.0 ± 8.6)	50	Surface (Flaws not obvious)
1066 (1950) 50 hours	636 ± 41 (89 ± 5.7)	11	Surface (Flaws not obvious)
1129 (2065) 140 hours	593 ± 36 (83 ± 5.0)	6	Surface Pits
1129 (2065) 240 hours	443 ± 58 (62.0 ± 8.1)	6	Surface Pits
1204 (2200) 24 hours	529 ± 19 (74.0 ± 2.6)	12	Surface Pits
1371 (2500) 24 hours	457 ± 29 (64 ± 4.1)	12	Surface Pits

with exposure at 1200°C (for times of 100 hr.) while others decreased for the same exposure conditions. Richerson and Yonushonis (15) have made similar observations on hot-pressed, silicon nitride. More recently, the combined effect of flaw healing and pit formation was demonstrated by Jones and Rowcliff (22), for silicon nitride exposed at temperatures of 1370°C for periods up to 64 hours. For both indented (knoop; 1 Kg) and transverse ground specimens, the strength first increased then decreased as the exposure time increased (Figure 13).

Reaction bonded silicon nitride behaves in a manner quite different from that of the hot-pressed material. Flaw healing results in a significant strength increase in this material at elevated temperatures. When the material is cooled to room temperature, however, much of this increase is lost as a result of surface cracking caused by a phase transformation of cristobalite in the oxide coat that forms on the surface at high temperatures (27). The absence of strength degradation (at 1200°C)

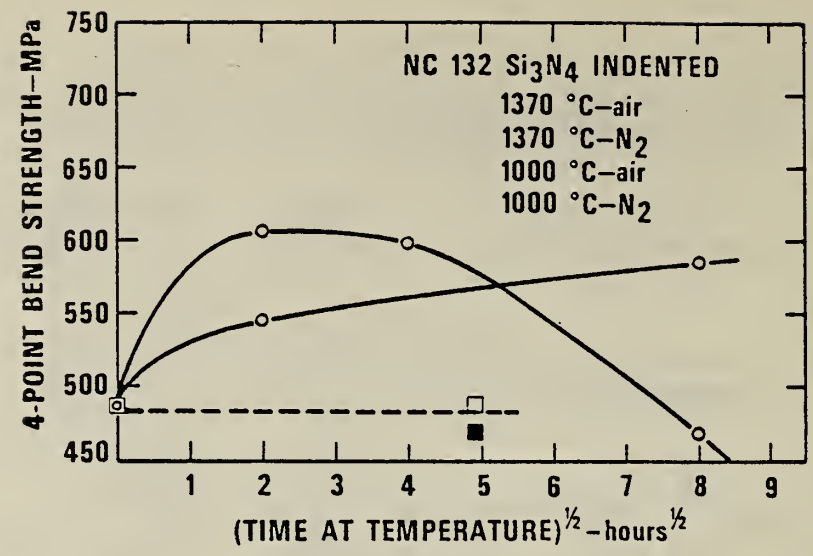

Figure 13. Effect of high temperature exposure on the strength of silicon nitride (NC132) measured at room temperature (from ref. 22).

after sustained (1000 hr.) exposures (28), suggests that pit formation and subcritical crack growth are not significant factors limiting the lifetime of this material.*

LIFETIME ESTIMATE: EFFECT OF FLAW HEALING AND PIT FORMATION

From the above discussion, we conclude that flaw healing, pit formation and subcritical crack growth must be considered simultaneously in order to establish an accurate method of lifetime prediction. The development of a failure prediction method requires each of these processes to be evaluated independently. Once they have been characterized, mathematical techniques can be used to determine the relative contribution of each of these processes to the total failure time.

Subcritical crack growth can be characterized either by strength or fracture mechanics techniques. However, when flaw healing or pit formation is occurring, the use of strength techniques for evaluating crack growth parameters may not be a good procedure, since both of these processes have an independent effect on the material's strength. The feasibility of quantifying the crack growth rate by fracture mechanics techniques has been demonstrated by Evans and Wiederhorn (30), who have shown that

*Recently, Richerson et al. (29) have observed pit formation in heavily oxidized reaction bonded silicon nitride.

the crack velocity can be represented as a power function of the applied stress intensity factor (Equation 1). Details on the application of fracture mechanics techniques to crack growth data can be found in ref. 31.

A second method of collecting crack velocity data was illustrated recently by Rowcliff (22), who used 3 point bend specimens to study the static fatigue of silicon nitride and silicon carbide. The specimens were all indented to form well-characterized cracks in the tensile surface of the specimens. The technique is based on the assumption that equation 1 is the correct form of the crack velocity equation. By rearranging Equation 2, the following equation is obtained for the failure time, t, of a component that is subjected to a constant applied load

$$t = \frac{2a_i}{(n-2)v_i} \tag{11}$$

Thus, by measuring the initial crack size, a_i, and the time to failure, t, the initial crack velocity, v_i, can be determined. The stress intensity factor that corresponds to v_i is obtained directly from a_i ($K_{Ii} = \sigma Y\sqrt{a_i}$)*.

Data on flaw healing or on pit formation can be obtained from strength measurements. Data on magnesia-doped, hot-pressed silicon nitride and reaction bonded silicon nitride suggest that crack healing occurs relatively quickly and is completed before pits begin to form in the component surface. Therefore, strength changes during the early stages of component exposure can be used to characterize the crack healing process; strength changes occurring after extended exposure can be used to characterize the pit formation process. For normally machined surfaces, quantification of both of these processes requires the collection of extensive strength data so that the strength distribution can be determined accurately as a function of exposure time.

Data on hot-pressed silicon nitride suggests that both the mean strength and its standard deviation change with exposure time when flaw healing occurs (20,24,25). In terms of a Weibull distribution, Equation 4, both the Weibull strength, S_o, and the shape parameter, m, are a function of time. Data on reaction bonded silicon nitride suggests that only S_o is a function of

*The validity of the data obtained by this technique is limited by the assumption that the crack size at failure is small relative to the specimen dimensions. As has already been noted, this same limitation applies to earlier parts of this paper.

time (28). The effect of flaw healing on specimens that contain large initial cracks can be determined from studies on specimens that have been indented so that relatively large cracks are introduced into the specimen surface. Studies of this type have been conducted recently by Tighe and Wiederhorn (20,24) and by Cubicciotti et al. (22). The investigation by Singhal et al. (25) of strength degradation after long term exposure suggests that for both crack healing and pit formation S_o and m seem to approach fixed values after a certain amount of time, so that both distributions eventually become stable with regard to further exposure.

Once crack growth, flaw healing, and pit formation have been quantified, the combined failure probability, and the total time to failure can be estimated. To obtain these estimates it is necessary to develop a procedure to determine which mechanism controls failure at a given probability level. Flaw healing and pit formation as a combined failure mechanism will be discussed first. For simplicity it is assumed that the Weibull slope, m_1, for crack healing is less than the Weibull slope, m_2, for pit formation, and that m_1 and m_2 do not depend on time. The Weibull strength for crack healing, S_1, and that for pit formation, S_2, are assumed to follow exponential decay curves that can be fit to the following formulae:

$$\text{(flaw healing)} \qquad S_1 = S_{o_1} + \Delta S_{o_1}(1-\exp(-\alpha t)) \qquad (12)$$

$$\text{(pit formation)} \qquad S_2 = S_{o_2} - \Delta S_{o_2}(1-\exp(-\beta t)) \qquad (13)$$

where S_{o_1}, S_{o_2}, ΔS_{o_1}, ΔS_{o_2}, α and β are determined from experimental strength data. The initial Weibull strengths for flaw healing and pit growth are S_{o_1} and S_{o_2} respectively, while ΔS_{o_1} and ΔS_{o_2} are the changes in strength for these two processes after extended exposure times. α and β determine the rate at which these changes in strength occur. If Equations 12 and 13 are substituted into Equation 4, time dependent strength distributions are obtained that describe the effect of exposure time on strength.

The type of behavior expected from Equations 12 and 13 is shown schematically in Figure 14. We see that during the initial stages of exposure, failure is determined entirely by the initial flaw population, while in the later stages of exposure, pit formation dominates the strength distribution. At any point in time, the combined failure probability, F, is given by the following relation (32):

$$(1-F) = (1-F_1)\ (1-F_2) \qquad (14)$$

where F_1 and F_2 are the time dependent failure probabilities for flaw healing and pit formation respectively. Thus, a unique

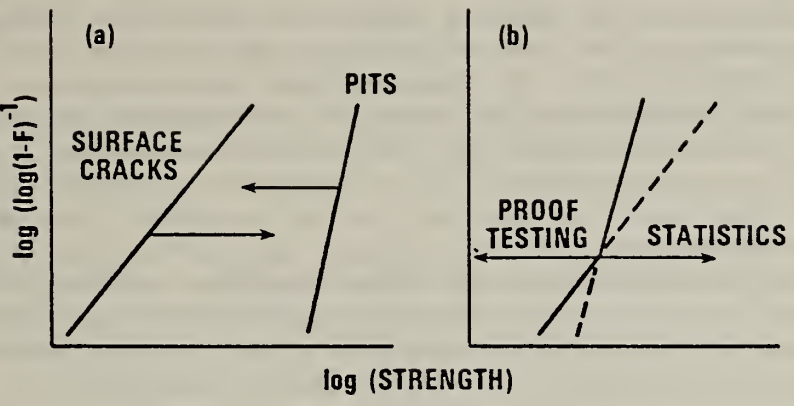

Figure 14. Schematic representation of the effect of high temperature exposure on the strength distribution: (a) initial strength distribution. Curves are assumed to move in the direction of the arrows as the exposure time is increased; (b) distribution after the flaw structure has reached a state of "equilibrium". Proof testing or nondestructive evaluation can be used to improve reliability at stresses lower than the point of intersection of the two lines, statistics can be used to the right of the point of intersection.

equation is obtained that relates the failure strength, S, to the failure probability, F.

With regard to lifetime prediction, the above discussion is sufficient to draw several important conclusions with regard to proof testing and nondestructive testing. At any time during exposure, the strength of components to the left of the point of intersection of the two curves shown in Figure 14 will be controlled by the initial flaw population. Those specimens that lie to the left of the intersection will contain the largest flaws and consequently will be the ones to be eliminated by proof testing or nondestructive inspection. Since the initial flaw population controls the strength in this regime, proof testing and nondestructive evaluation techniques can be used to truncate the population, and the theory presented earlier in this paper can be used to provide a conservative estimate of the component lifetime. The intersection of the two curves shown in Figure 14 provides an upper limit to the proof test load that can be usefully employed to truncate the initial flaw population. Above this load, component strength depends not on the flaws initially present in

the component, but on those that are generated by exposure to elevated temperatures (20,24).

After long periods of exposure, proof testing or nondestructive evaluation can be applied again over the entire range of strengths provided the flaw distribution (pits and cracks) has reached a static state. If, however, the distribution to the right of the intersection in Figure 14 represents a dynamic state of equilibrium, then new pits will be continuously generated as the old ones are removed. As a consequence, nondestructive evaluation and proof testing will not be a viable lifetime prediction technique. For the dynamic equilibrium situation, statistical techniques such as those described earlier in this paper would have to be used for purposes of lifetime prediction. Pits generated by the oxidation process would serve as the initial flaw distribution for the lifetime prediction.

The combined effects of subcritical crack growth and pit formation on strength can be determined by considering the rate at which each of these processes degrade the strength. As long as strength degradation due to pit formation exceeds that resulting from crack growth, subcritical crack growth will not play a major role in the strength degradation process; when the converse is true, crack growth will dominate the strength degradation process. The switch from one controlling mechanism to the other will occur when the two strength degradation rates are equal.

The rate of strength degradation due to pit formation can be determined by substituting S_2 of equation 13 for S_o of Equation 4, and differentiating with respect to time:

$$dS/dt = -\beta\ \Delta S_{o_2} [\exp(-\beta t)]\ [\ln(1-F)^{-1}]^{1/m} \qquad (15)$$

The rate of strength degradation due to crack growth has been derived by Fuller et al. (4) and is given by the following expression:

$$dS/dt = -\ (AY^2 K_{IC}{}^{n-2}/2)\ (\sigma/S)^n S^3 \qquad (16)$$

where A and n are defined by equation 1; Y is a geometric constant; σ is the applied stress and S is the instantaneous strength. Equating Equations 15 and 16, and substituting Equations 4 and 13 for S, an equation can be obtained which gives the time, t_p, at which the mechanism of strength degradation changes from pit formation to crack growth. The total time to failure is then equal to t_p, plus the time, t_c, for the crack to grow to a critical size. t_c can be determined from Equation 2, (using Equations 4 and 13 to evaluate the strength at which the degradation mechanism changes from pit formation to crack growth).

Although the mathematical scheme for obtaining the total time to failure is straightforward, the equations are not included here because of their complexity. Never-the-less, the procedure does provide a rational method of obtaining the total time to failure when pit formation plays a critical role in determining component lifetime. It is worth noting that the final equation can be expressed in terms of strength, probability and failure time. This type of representation was first suggested by Davidge et al. (33) as a method of design with ceramic materials.

SUMMARY

In this paper, a review is presented of current techniques used to evaluate the lifetime capability of structural ceramics. Three successful applications of these techniques are presented and discussed in order to demonstrate the viability of the techniques for purposes of engineering design. Finally, limitations of the techniques are discussed with regard to heat-engine applications. An extension of theory is recommended to treat crack healing and pit formation resulting from high temperature exposure.

The theory presented in this paper is based on the theory of linear-elastic, fracture mechanics. Failure of structural ceramics is assumed to be the result of subcritical crack growth from pre-existing flaws in the structural components. Lifetime predications require evaluation of the initial flaw size and of the rate at which cracks grow when subjected to applied loads. The three techniques that can be used to evaluate the initial flaw size are nondestructive evaluation, proof-testing and statistics, while the three techniques that can be used to evaluate the rate of crack growth are fracture mechanics techniques, static fatigue techniques (stress rupture) and dynamic fatigue techniques (constant loading rate to failure). The critical equations required for purposes of failure prediction are presented in the paper. Successful applications of the lifetime prediction method are illustrated for electronic-substrate ceramics, for vitreous grinding wheels and for high-purity aluminum oxide at elevated temperatures.

Potential limitations in applying the technique to heat engine ceramics, such as silicon nitride and silicon carbide, are discussed. These limitations arise because of flaw generation and flaw healing that is observed to occur in these materials at elevated temperatures. Flaw generation can be caused by a number of processes: oxidation or other environmental attack which results in surface pit formation, particle impact or component contact which results in localized stresses that nucleate cracks, and thermal shock which results in transient stresses that can result in crack formation. Flaw healing can

be attributed to surface dissolution caused by oxidation and silicate glass formation. These processes change the initial flaw population so that failure no longer occurs from machining flaws originally present in the ceramic. In this situation the development of a model for failure prediction requires the consideration of flaw generation processes.

Extension of the theory presented in earlier sections of the paper is illustrated for the combined processes of flaw healing, pit formation and subcritical crack growth. The method independently evaluates these three processes and then determines the relative contribution of each of these processes to the total failure time. Conditions are established for proof testing of as-received components. Because of the occurrence of pit formation, a maximum value for the proof test load is established, above which proof testing does not contribute to component reliability. After long term exposure, proof testing or nondestructive evaluation can be applied again provided the flaw (pit) distribution has reached a state of static equilibrium. If, however, the flaw distribution has reached a state of dynamic equilibrium, then statistical techniques must be applied for lifetime prediction. Assuming that the strength distribution of pits can be represented by a two parameter Weibull distribution, the application of statistics is discussed for the combined failure modes of pit formation and crack growth. For these conditions, equations are developed for determining the total failure time.

ACKNOWLEDGEMENTS:

One of the authors (JER) is pleased to acknowledge the support of the Office of Naval Research, Metallurgy and Ceramics Program, the other authors are pleased to acknowledge the support of the Department of Energy, Division of Fossil Fuel Utilization.

REFERENCES

1. A.G. Evans and S.M. Wiederhorn, "Proof Testing of Ceramic Materials-An Analytical Basis for Failure Prediction," Int. J. Fract., 10, 379-92 (1974).
2. S.M. Wiederhorn, "Reliability, Life Prediction, and Proof Testing of Ceramics," pp. 635-65 in Ceramics for High Performance Applications, ed. by J. J. Burke, A.E. Gorum, and R.N, Katz, Brook Hill Pub. Co., Chestnut Hill, MA. (1974).

3. J.E. Ritter, Jr., "Engineering Design and Fatigue Failure of Brittle Materials," pp. 667-686 in Fracture Mechanics of Ceramics, Vol. 4, ed. by R.C. Bradt, D.P.H. Hasselman, and F. Lange, Plenum Press, NY (1978).
4. S.M. Wiederhorn, E.R. Fuller, Jr., J.E. Ritter, Jr., and P.B. Oates, "Proof Testing of Ceramics: I. Experiment" NBSIR 79-1934; "II Theory," NBSIR 79-1944, (December 1979).
5. J.E. Ritter, Jr. and J.N. Humenik, "Static and Dynamic Fatigue of Polycrystalline Alumina," J. Mat. Sci., 14, 626-632 (1979).
6. J.N. Humenik and J. E. Ritter, Jr., "Susceptibility of Alumina Substrates to stress Corrosion Cracking During Wet Processing," to be published, Bull. Am. Ceram. Soc.
7. J.E. Ritter, Jr. and S.A. Wulf, "Evaluation of Proof Testing to Assure Against Delayed Failure," Bull. Am. Ceram. Soc. 57, 186-190 (1978).
8. K. Jakus, T. Service, and J.E. Ritter, Jr., "High Temperature Fatigue Behaviour of Polycrystalline Alumina," to be published, J. Am. Ceram. Soc.
9. S.M. Wiederhorn, E.R. Fuller, Jr., J. Mandel, and A.G. Evans, "An Error Analysis of Failure Prediction Techniques Derived from Fracture Mechanics," J. Am. Ceram. Soc. 59, 403-11 (1976).
10. D. F. Jacobs and J.E. Ritter, Jr., "Uncertainty in Minimum Lifetime Predictions," J. Am. Ceram. Soc. 59, 481-486 (1976).
11. P.N. Thorby, "Experimental Errors in Estimating Times to Failure," J. Am. Ceram. Soc. 59, 514-16, (1976).
12. S.M. Wiederhorn, "Dependence of Lifetime Predictions on the Form of the Crack Propagation Equation," pp. 893-901 in Fracture 1977, Vol. 3, D.M.R. Taplin, Ed., University of Waterloo Press, Waterloo, Ontario, Canada (1977).
13. R.W. Rice, S.W. Freiman, and J.J. Mecholsky, Jr., "Fracture Sources in Si_3N_4 and SiC," pp. 665 in Proceedings of the 1977 DARPA/NAVSEA Ceramic Gas Turbine Demonstration Engine, J.W. Fairbanks and R.W. Rice, Eds., Metal and Ceramics Information Center Report MCIC-78-36, Battelle Columbus Laboratories, Columbus, Ohio (1978).
14. S.W. Freiman, C. Cm. Wu, K.R. McKinney, and W.J. McDonough, pp 655-663 in ref. 13.
15. D.W. Richerson and T.M. Yonushonis, "Environmental Effects on the Strength of Silicon-Nitride Materials," pp. 247-71 in ref. 13.
16. F.F. Lange, "Evidence for Cavitation in Crack Growth," J. Am. Ceram. Soc. 62 222-3 (1979).
17. N.J. Tighe, "Structure of Slow Crack Interfaces in Silicon Nitride," J. Mater. Sci. 13, 1455-63 (1978).

18. S.W. Freiman, A. Williams, J. J. Mecholsky and R.W. Rice, "Fracture of Si_3N_4 and SiC," pp. 824-34 in Ceramic Microstructures '76, R.M. Fulrath and J.A. Pask, Eds., Westview Press, Boulder, Colo. (1977).
19. S.W. Freiman, J.J. Mecholsky, W.J. McDonough, and R.W. Rice, "Effects of Oxidation on the Room Temperature Strength of Hot-Pressed Si_3N_4-MgO and Si_3N_4-ZrO_2," pp. 1069-76 in Ceramics for High Performance Applications," J.J. Burke, E.M. Lenoe, and R.N. Katz, Brook Hill Publishing Co., Chestnut Hill, Mass. (1978).
20. S.M. Wiederhorn and N.J. Tighe, "Proof-Testing of Hot-Pressed Silicon Nitride," J. Mat. Sci. 13, 1781-93 (1978).
21. D. Cubicciotti and K.H. Lau, "Kinetics of Oxidation of Hot Pressed Silicon Nitride Containing Magnesia," J. Am. Ceram. Soc., 61 512-7 (1978).
22. D.D. Cubicciotti, R.L. Jones, K.H. Lau, and D.J. Rowcliffe, "High Temperature Oxidation and Mechanical Properties of Silicon Nitride," Interim Scientific Report 5522-2, Nov. 15, 1978, Prepared for Air Force Office of Scientific Research/NE, SRI International.
23. T.M. Yonushonis and D.W. Richerson, "Strength of Reaction-Bonded Silicon Nitride," pp.219-233 in ref. 13.
24. S.M. Wiederhorn and N.J. Tighe, "Effect of Flaw Generation on Proof-Testing," pp 689-700 in ref. 13.
25. A.F. McLean, E.A. Risher, R.J. Bratton and D.G. Miller, pp 133-134 in Brittle Materials Design, High Temperature Gas Turbine, technical report AMMRC CTR 75-28 to the Army Materials and Mechanics Research Center, Watertown, Mass., October 1975.
26. J.A. Rubin, "Probable Causes of Pitting in Hot-Pressed Si_3N_4 Ceramics," pp. 739-743 in ref. 13.
27. R.W. Davidge, A.G. Evans, A.G. Gilling and P.R. Wilgman, "Oxidation of Reaction Sintered Silicon Nitride and Effects on Strength," in Special Ceramics, 5, 329-44 (1972).
28. N.J. Tighe, to be published.
29. D.W. Richerson, private communication.
30. A.G. Evans and S.M. Wiederhorn, "Crack Propagation and Failure Prediction in Silicon Nitride at Elevated Temperatures," J. Mat. Sci., 9, 270-278 (1974).
31. A.G. Evans, "Fracture Mechanics Determinations," pp.17-48 in Fracture Mechanics of Ceramics, Vol. 1, R.C. Bradt, D.P.H. Hasselman and F.F. Lange, eds., Plenum Press, New York (1974).
32. N.R. Mann, R.E. Shafer and N.D. Singpurwalla, Methods for Statistical Analysis of Reliability Data, John Wiley and Sons, New York (1974).

33. R.W. Davidge, J.R. McLaren and G. Tappin, "Strength-Probability-Time (SPT) Relationships in Ceramics," J. Mat. Sci. 8, 1699-1705 (1973).
34. N.J. Tighe and S.M. Wiederhorn, "Fracture of Brittle Materials at High Temperatures," Air Force Materials Laboratory Technical Report: AFML-TR-78-83, July 1978.

NBS-114A (REV. 9-78)

U.S. DEPT. OF COMM. BIBLIOGRAPHIC DATA SHEET	1. PUBLICATION OR REPORT NO. NBSIR 80-2047	2. Gov't. Accession No.	3. Recipient's Accession No.

4. TITLE AND SUBTITLE

APPLICATION OF FRACTURE MECHANICS IN ASSURING AGAINST FATIGUE FAILURE OF CERAMIC COMPONENTS

5. Publication Date: June 1980

6. Performing Organization Code

7. AUTHOR(S)

E. R. Fuller, Jr.
J. E. Ritter, Jr., S. M. Wiederhorn, N. J. Tighe, and

8. Performing Organ. Report No.

9. PERFORMING ORGANIZATION NAME AND ADDRESS

NATIONAL BUREAU OF STANDARDS
DEPARTMENT OF COMMERCE
WASHINGTON, DC 20234

10. Project/Task/Work Unit No.

11. Contract/Grant No.

12. SPONSORING ORGANIZATION NAME AND COMPLETE ADDRESS *(Street, City, State, ZIP)*

Department of Energy
Fossil Fuel Utilization Division
Washington, D.C.

13. Type of Report & Period Covered

14. Sponsoring Agency Code

15. SUPPLEMENTARY NOTES

☐ Document describes a computer program; SF-185, FIPS Software Summary, is attached.

16. ABSTRACT *(A 200-word or less factual summary of most significant information. If document includes a significant bibliography or literature survey, mention it here.)*

This paper will review the application of fracture mechanics theory to the prevention of delayed failure of ceramics. Three successful applications of this theory of assuring the mechanical reliability of ceramics are discussed in order to demonstrate the viability of the theory for purposes of engineering design. Finally, a description is presented of practical limitations of the theory with regard to heat engine application. Methods of overcoming these limitations through modification of test procedures, and application of statistical theory are then presented.

17. KEY WORDS *(six to twelve entries; alphabetical order; capitalize only the first letter of the first key word unless a proper name; separated by semicolons)*

Dynamic fatigue; fracture mechanics; lifetime prediction; proof testing; stress corrosion; subcritical crack growth.

18. AVAILABILITY ☒ Unlimited

☐ For Official Distribution. Do Not Release to NTIS

☐ Order From Sup. of Doc., U.S. Government Printing Office, Washington, DC 20402, SD Stock No. SN003-003-

☒ Order From National Technical Information Service (NTIS), Springfield, VA. 22161

19. SECURITY CLASS (THIS REPORT)	21. NO. OF PRINTED PAGES
UNCLASSIFIED	33
20. SECURITY CLASS (THIS PAGE)	**22. Price**
UNCLASSIFIED	$6.00

USCOMM-DC